State-of-stress and stress rotations: Quantifying the role of surface topography and subsurface density contrasts in magmatic rift zones (Eastern Rift, Africa)

S.J. Oliva[1,2] (soliva@eoas.ubc.ca), C.J. Ebinger[1], E. Rivalta[2], C. Williams[3], C. Wauthier[4], C. Currie[5]

[1]Tulane University (USA), [2]*now at* University of British Columbia (Canada), [2]GFZ Center for Geosciences (Germany), [3]GNS Science (New Zealand), [4]Pennsylvania State University (USA), [5]University of Alberta (Canada)

1. Introduction

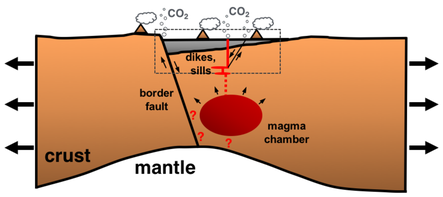

◄ **Figure 1.** Schematic diagram of a rift system with thinned crust (and mantle) and a sediment-filled basin flanked by a border fault. A dike and sill complex is sourced from a deeper magma chamber. Volcanoes and rift topography load the plate. CO_2 is degassed via volcanic conduits and percolation through faults.

- Rift topography, volcanoes, and underlying crustal magma chambers cause fundamental changes to the density structure, load the plates, and change the state-of-stress within the crust and mantle lithosphere
- **Objective:** to quantify the interactions between surface and subsurface loading on crustal state-of-stress in a rift setting
- **Key question:** ***How do surface (e.g., volcanoes, rift flanks) and subsurface intrusions (sills, dikes, magma chambers) combine with in-plane stresses in magmatic rift zones?***

2. Geographical background

▶ **Figure 2.** ***Map.***

- REGION: North Tanzania Divergence, southernmost sector of Eastern branch, East African Rift
- CRAFTI local array, 2013-2014 (blue circles)
- OL: Oldoinyo Lengai
- 2007-2008 seismomagmatic sequence (dike, earthquakes, OL eruption; dike labeled in green)

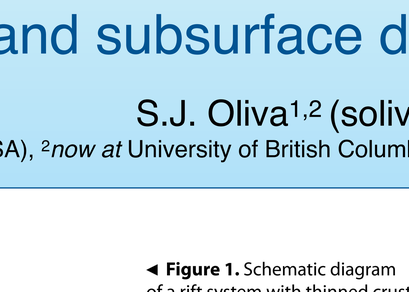

▶ **Figure 3.** ***Local stress rotation.***

- Summed moment tensors: local earthquakes 2013-2014 (blue); teleseisms 1964-2007 (black) (Craig et al., 2011)
- Green arrows: GPS velocity vectors for a Nubia-fixed model (King et al., 2019)
- ~60º local stress rotation in middle solid blue box
- Model domain for 2D: Cross-section along black dashed line
- Model domain for 3D: Blue dotted box, higher res inner box
- Receiver functions (Plasman et al., 2017) and joint seismic-gravity tomography (Roecker et al., 2017) constrain Moho/crustal thicknesses.

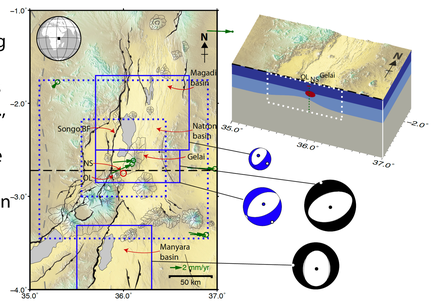

(Figures adapted from Oliva et al., 2019; Weinstein et al., 2017)

INPUT Constraints from tomography, refraction studies, geometry → **OUTPUT** Stress/Strain, Principal stress directions → **COMPARE** with earthquake locations, focal mechanisms, GPS models

3. Analytical modeling

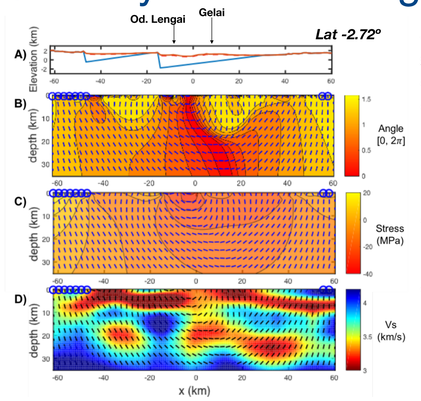

◄ **Figure 4.** ***2D analytical model of E-W cross-sections across the rift.***

- Topographic load + regional extension
- Preferred region for melt storage beneath the rift valley (red in B and C) that is enhanced compared to other parts of the Natron rift sector. Location matches hypothesized sills and tomography (D).
- Lines: direction of most compressive principal stress, proxy for likely direction of intrusion propagation
- (D) Corresponding shear wave (Vs) tomography transect: Low-Vs zones at about 20 km depth are interpreted as magma chambers (Roecker et al, 2017).

4. Numerical 2D modeling

▶ **Figure 5.** ***2D static models, E-W transects.***

- Using PyLith (Aagard et al., 2013)
- Topography (SRTM90) and estimated basin depths from refraction and wide-angle reflection data (Birt et al., 1997)
- Stresses = deviations in gravitational stress with respect to a reference model (uniform-thickness three-layer model with no magmatic systems)
- Numerical models of separate stress contributions of each rift component colored by displacement magnitude (proxy for stress and strain)
- Separate effects of d) surface topography, e) an intruded sill (density contrast), f) an inflating magma chamber (density contrast and outward pressure), g) the Moho topography of the thinned crust, h) combined effects of d-g, and i) combined effects of all plus a displacement boundary condition (regional extension)

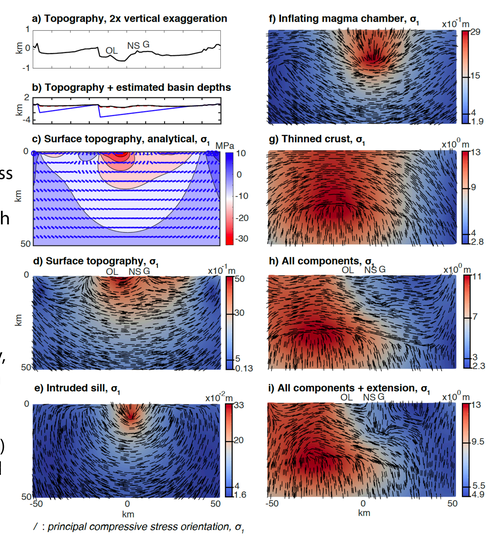

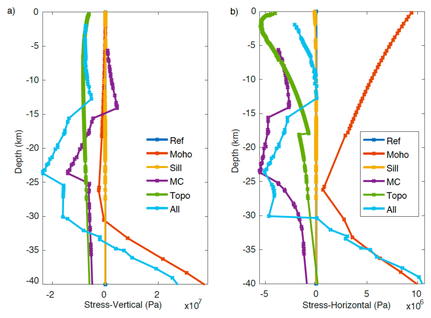

◄ **Figure 6.** ***1D profiles from 2D static models.***

- Vertical and horizontal stresses along the 1D depth profile (deviation from a reference model)
- Within 100 m of the profile (x=2750 m)
- Ref: reference, Topo: topography (Fig. 5d), Sill (Fig. 5e), MC: magma chamber (Fig. 5f), Moho: thinned crust (Fig. 5g), All (Fig. 5h).
- Topography has the largest effect close to the surface; the magma chamber inflation has a large effect nearby but becomes negligible farther away
- Horizontal stresses are an order of magnitude smaller than vertical stresses.

5. Numerical 3D modeling

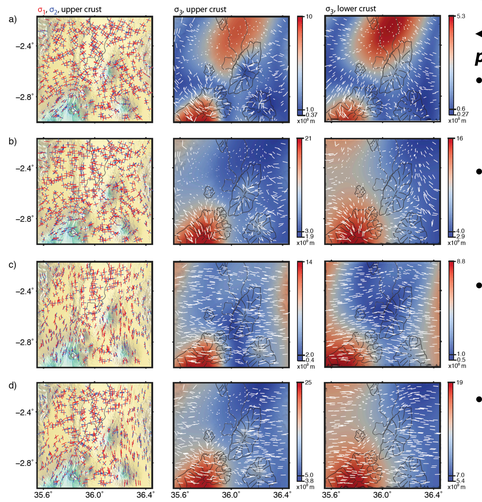

◄ **Figure 7.** ***Map view of principal stresses.***

- a) Topography only, b) all components together, c) topography + extension, and d) all components + extension
- Topography with subsurface effects produces a NNW-SSE sigma3 ~ T-axis from stress inversion of local and teleseismic earthquakes
- Modulation of the extension imposed on the models could produce stress orientations similar to those observed from focal mechanisms
- Extension rotates preferred intrusion orientation (sigma1-sigma2 plane) to near-vertical in Southern Gelai

▼ **Figure 8. Schematic diagram of early-stage rifting.**

- In addition to topographic loading, the subsurface density gradients from a thinned crust and the crustal magmatic complex also alter the stress field at depth
- GPS: constrain surface motions; Seismicity: stress (strain) field at depth
- Surface topography and extension influences the shallow stress field the most (~upper crust), but at depth (~lower crust), subsurface density contrasts play a larger role.
- Local stress field due to rift magmatic system (surface and subsurface) determine orientation and evolution of transfer fault systems
- Large subsurface stresses may be overlooked when only considering surface-motion constraints but are key to a holistic three-dimensional understanding of rift tectonics

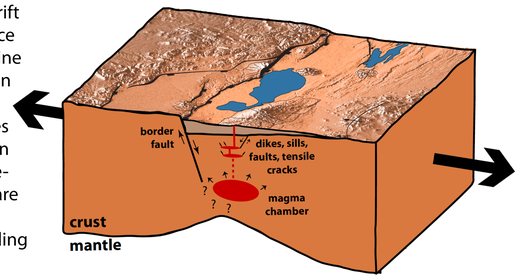

Acknowledgments

This work has been supported by a GSA student research grant that enabled a research visit in GFZ Centre for Geosciences (Germany), as well as CIG student travel support to attend for PyLith training. The work was performed using MATLAB, PyLith, Trelis, as well as ParaView for visualization, and using high performance computing resources at Tulane University.

References

Aagaard et al., A domain decomposition approach to implementing fault slip in finite-element models of quasi-static and dynamic crustal deformation, *J. Geophys. Res.: Solid Earth, 118*(6), 3059-3079, 2013.

Birt et al., The influence of pre-existing structures on the evolution of the southern Kenya Rift Valley—evidence from seismic and gravity studies, *Tectonophys., 278*(1), 211-242, 1997.

Craig et al., Earthquake distribution patterns in Africa: their relationship to variations in lithospheric and geological structure, and their rheological implications, *Geophys. J. Int., 185*(1), 403-434, 2011.

King et al., GPS velocity field (MIT 2019.0) for the East African Rift system generated by King et al., 2019 URL: http://doi.iedadata.org/324785, doi:10.1594/IEDA/324785.

Oliva et al., Insights into fault-magma interactions in an early-stage continental rift from source mechanisms and correlated volcano-tectonic earthquakes, *Geophys. Res. Lett., 46*(4), 2065-2074, 2019.

Plasman et al., Lithospheric low-velocity zones associated with a magmatic segment of the Tanzanian Rift, East Africa.,*Geophys. J. Int., 210*(1), 465-481, 2017.

Roecker et al., Subsurface images of the Eastern Rift, Africa, from the joint inversion of body waves, surface waves and gravity: investigating the role of fluids in early-stage continental rifting, *Geophys. J. Int., 210*(2), 931-950, 2017.

Tiberi et al., Lithospheric modification by extension and magmatism at the craton-orogenic boundary: North Tanzania Divergence, East Africa, *Geophys. J. Int.*, submitted.

Weinstein et al., Fault-magma interactions during early continental rifting: seismicity of the Magadi-Natron-Manyara basins, Africa, *Geochem. Geophys. Geosys. 18*(10), 3662-3686, 2017.